


Spectroscopic investigations on PVDF-Fe₂O₃ nanocomposites

Dorina Chipara,¹ Victor Kuncser,² Karen Lozano,³ Mataz Alcoutlabi,³ Elamin Ibrahim,⁴ Mircea Chipara ¹

¹Department of Physics and Astronomy, The University of Texas Rio Grande Valley, Edinburg, Texas

²Laboratory of Magnetism and Superconductivity, National Institute of Materials Physics, Magurele, Bucharest, Romania

³Department of Mechanical Engineering, The University of Texas Rio Grande Valley, Edinburg, Texas

⁴Department of Chemistry, The University of Texas Rio Grande Valley, Edinburg, Texas

Correspondence to: M. Chipara (E-mail: mircea.chipara@utrgv.edu)

ABSTRACT: Polyvinylidene fluoride-iron oxide (PVDF-Fe₂O₃) nanocomposites have been obtained by melt mixing of PVDF with Fe₂O₃ nanoparticles. The interactions between the polymeric matrix and the nanofiller have been investigated by wide angle X-ray scattering (WAXS), Fourier transform infrared spectroscopy (FTIR), and Raman spectroscopy, using both red and green excitations (lasers). WAXS, FTIR, and Raman spectra confirm that all samples contain α PVDF as the major crystalline form of the polymeric matrix. Experimental data revealed small changes in the positions of X-ray lines as well as modifications of the width of X-ray lines upon loading by Fe₂O₃ nanoparticles. FTIR and Raman spectra are dominated by the lines of the polymeric matrix. Within the experimental errors, the positions of Raman lines are not affected by the wavelength of the incoming electromagnetic radiation, although they are sensitive to the strain of the polymeric matrix induced by addition of the nanofiller. The loading of the polymeric matrix with nanoparticles stretches the macromolecular chains, affecting their vibrational spectra (FTIR and Raman). A complex dependence of the positions of some Raman and FTIR lines on the loading with Fe₂O₃ is reported. The manuscript provides a detailed analysis of the effects of nanofiller on the position of WAXS, FTIR, and Raman lines. © 2020 Wiley Periodicals, Inc. *J. Appl. Polym. Sci.* **2020**, *137*, 48907.

KEYWORDS: composites; phase behavior; nanoparticles; nanowires and nanocrystals; spectroscopy; X-ray

Received 17 July 2019; accepted 28 November 2019

DOI: 10.1002/app.48907

INTRODUCTION

Polyvinylidene fluoride (PVDF) is a thermoplastic semicrystalline polymer. Due to the presence of F atoms, PVDF is susceptible to form hydrogen bonds within the same macromolecular chain, between neighboring macromolecular chains or with other adjacent (hydrogen) atoms. Fluorine atoms are expected to attract neighboring electrons, disturbing their spatial distribution. PVDF has up to five crystalline structures labeled from α to ϵ ^{1,2}; the most common is the α PVDF, which is characterized by the symmetrical distribution of fluorine atoms and hence is not ferroelectric. There are only three well-established crystalline structures labeled as β , γ , and δ that exhibit ferroelectric, piezoelectric, and pyroelectric features^{3,4} related to the nonsymmetrical distribution of fluorine atoms.

The loading of the PVDF matrix by magnetic nanoparticles may trigger a coupling between magnetic features of the nanofiller and the electric characteristics of the matrix, leading to a ferroic material. Such materials belong to^{5–7} a novel class of materials with new features. Polymer-based ferroics will have lightweight

and elastic features desirable in many potential applications added to their (coupled) magnetic and electric characteristics.

PVDF has the melting transition temperature in the range of 150–160 °C.⁸ The exact value depends weakly on the nature of the crystalline phase. Melting peak at 171 and 180 °C have been reported² for the α and β phase of PVDF, respectively. The amorphous component of PVDF is responsible for the glass transition, typically located at about –35 °C.^{9,10}

The availability of lasers had a huge effect on the development of Raman spectroscopy. Thus, in the period 1950–2000, the Raman spectra of most commercially available polymers were reported elsewhere.^{11–13} While the resolution of these spectrometers was about 10 cm⁻¹, the positions of Raman lines and the assignment of recorded spectra were typically accurate. However, the details regarding the width of the Raman lines and their shape were determined with significant errors, forcing many authors to restrict their analysis to the position of Raman lines. The new generation of detectors coupled with the improvements of laser diodes resulted in new Raman spectrometers with resolutions of

the order of 1 cm^{-1} . Such enhanced resolutions triggered a renewed interest in the study of polymers with particular emphasis on polymer-based nanocomposites.^{14,15} In the case of polymer-based nanocomposites, the loading of the polymeric matrix by the nanofiller stretches the macromolecular chains. This was expected to affect the atomic and molecular vibrations, as sensed by Raman and FTIR spectroscopy. Another recent area of research is represented by polymer nanofibers.^{16,17}

Subsequent Raman studies revealed that the external stress/strain affects the phase transitions in PVDF,¹⁸ that the loading of PVDF matrices with nanofillers disturb the crystalline phases and the phase transitions of PVDF^{2,9} and added Raman spectroscopy to the list of experimental techniques that can sense phase transition in PVDF.¹⁹ As of now, it is recognized that the mechanical stress or strain may affect the position of some Raman lines²⁰ and that the shift of the position of the Raman line is proportional to the stress (assuming that the polymer is in the high elastic state, i.e., obeys a linear stress–strain dependence).^{20–22} However, there is not an accepted understanding of the effect of stress on the width of Raman lines or their shape.²³ As the width and shape of such spectra require a certain number of experimental points, we may speculate that the actual accuracy of Raman spectrometer makes this task difficult. The next experimental effort will focus on the calibration of the shift–stress or shift–strain dependencies.

Both Raman and FTIR spectroscopies are sensing atomic and molecular motions. In the case of Raman spectroscopy, the detection wavelength is at any wavelength excepting the wavelength of the incident electromagnetic radiation, while in FTIR spectroscopy, the two wavelengths are identical. Both spectroscopies focus on the same range of wavelengths, typically starting from 100 to about 4000 cm^{-1} . The consequence of this difference is that FTIR spectra are associated with motions that change the dipole moment while the Raman spectra are due to motions that modify the polarizability of the sample. Consequently, there are common lines (observed both in Raman or FTIR usually at the same position) as well as individual lines (recorded solely in Raman or in FTIR). Such pure vibrations (motions) are not usually observed in polymers, where the crowding of neighboring atoms is responsible for interactions that make complex the atomic and molecular motions. As a result, many lines have been noticed both in Raman and FTIR spectroscopy. As a natural extension, the effect of strain on the position of FTIR lines (in polymeric materials) has been reported.

For polymer-based nanocomposites, the expected outcome of this “common feature” is the dependence of the FTIR line position on the local stress, that is, in the case reported on the loading with nanofiller. FTIR and Raman data are supporting this hypothesis; nevertheless, in polymer-based nanocomposites, the shift of the Raman lines’ positions (of the matrix or the filler) was found to depend on the concentration of the nanofiller.^{24,25}

Maghemite (or $\gamma \text{ Fe}_2\text{O}_3$) is a ferrimagnetic iron oxide with a high Neel temperature, semiconducting features, and a ferrite spinel structure, considered to be nontoxic and biocompatible.

Wide angle X-ray scattering (WAXS) technique was developed as an X-ray diffraction technique for powders, where crystallites are

randomly distributed in space. The technique is frequently used in polymers, where the polymeric crystallites are usually randomly distributed.²⁶ Large area detectors are more and more frequently used to investigate polymers characterized by the preferential orientation of crystallites.²⁷ WAXS is frequently used to assess the crystal structure (composition)²⁶ and eventually the degree of crystallinity²⁸ of various polymers and polymer-based nanocomposites, including PVDF^{29,30} based materials.

WAXS linewidth is affected by several factors; the most important are the size of crystallites L and the strain exerted on the unit crystal. The first contribution is modeled by the Scherrer equation^{26,31,32}:

$$\omega_{S(hkl)}(2\theta) = \frac{C\lambda}{L_{hkl}\cos\theta} \quad (1)$$

where ω_s is the width of the line including the effect of the crystallite’s size, C is a constant, λ is the wavelength of the incoming X-ray wave, L is the length of the crystallite, h , k , l are integers that define the reflection plane, and θ is the reflection angle. It is important to recognize that L and the reflection angles are controlled by the type of the crystal and by the integers h , k , and l associated with the reflection considered. For a given reflection (or set of reflections), the changes in θ due to the crystallites’ size are small (as in most cases θ is ranging between 0 and 180° , so that $\cos\theta$ is positive for all considered reflections).

The other contribution to the linewidth, ω_ε , comes from the strain ε of the crystal unit and is described by³³:

$$\omega_\varepsilon(2\theta) = 4\varepsilon\tan\theta \quad (2)$$

where ω_ε is the width of the line, including the effect of the strain for a reflection measured at the angle 2θ , in most cases, the actual line width of the line measured at 2θ is the sum of these contributions.

The total broadening of the WAXS line, ω , is³³:

$$\omega = (\omega_{S(hkl)}^2 + \omega_\varepsilon^2 + \omega_0^2)^{\frac{1}{2}} \quad (3)$$

where ω_0 is the instrumental broadening.

In the case of polymer-based nanocomposites, the loading of the crystalline polymeric matrix may have two main effects on the WAXS spectrum of the matrix; the shifting of the X-Ray reflections indicating a change of the distance between the crystal’s atoms and the change of the width of the X-ray line, reflecting the combined effect of stress/strain exerted on the crystal and of the size of the (polymer) crystallite. If the changes in the distance between atoms are not large, it is possible to assume that the crystallites are preserving their structure, and consequently, these changes will contribute solely to the width of the WAXS lines and will not affect significantly their position. This is the framework within which WAXS data are discussed and analyzed.

Recent studies revealed that the position of the Raman line is affected by the strain of the polymeric matrix.^{34,35} In polymer-based nanocomposites, the positions of the Raman lines assigned to both the (nano)filler and polymeric matrix may shift due to the external strain (or by the strain generated during the loading

with the nanofiller of the polymer matrix). For example, in polymers filled with single-walled carbon nanotube (SWCNT) and subjected to strain (up to 1%), the increase of the strain results in the (linear) shift of the 2D line (located at about 2610 cm^{-1}) assigned to SWCNTs toward lower positions.³⁶ Similar results were obtained for epoxy-SWCNT nanocomposites, by monitoring the line located at about 2615 cm^{-1} assigned to the nanofiller.³⁷ The data regarding the effect of strain on the radial breathing mode of SWCNTs dispersed within epoxy resin are instrumental in the understanding of this behavior. For example, the lines located at 210 and 232 cm^{-1} show an increase of the position of the Raman line as the strain is increased, while the lines located at 268 and 272 cm^{-1} show a decrease of the position of the Raman lines as the strain is increased.³⁸ For these samples, the position of the G' Raman line is shifted to lower values as the strain is increased.³⁸

Typically, an elongation strain shifts the Raman lines of the polymer matrix towards smaller Raman shifts,³⁹ while a compressive strain is responsible for the shift of the Raman lines towards larger Raman shifts. This shift is proportional to the strain in the Hooke region,⁴⁰ where the stress is proportional to the strain. The effect of the mechanical strain/stress on the width of Raman lines was not yet fully understood, and consequently, the research will focus solely on the Raman line position.

The manuscript describes an investigation of polyvinylidene fluoride-iron oxide (PVDF- Fe_2O_3) nanocomposites by spectroscopic techniques (WAXS and Raman).

EXPERIMENTAL METHODS

Maghemite nanoparticles with the diameters ranging between 20 and 40 nm and PVDF were purchased from Alfa Aesar (Tewksbury, United States) and used as received. The nanocomposites were prepared by melt mixing, using a Haake PolyLab system with two counter-rotating screws. The melt mixing was performed in three stages the first one at 190°C and 60 rot/min for 30 min, the second one at 210°C and 80 rot/min for 15 min, and the last one at 180°C and 60 rot/min for 30 min. No degradation of the polymeric matrix was noticed (by WAXS, FTIR, and Raman).

WAXS spectra have been recorded by using a Bruker Discovery-8 spectrometer. FTIR data were performed by using a Tensor 27/Hyperion system from Bruker, operating in the ATR mode. Raman measurements have been carried out with a Renishaw InVia confocal microscope operating at 532 (green) and 785 (red) nm, respectively.

EXPERIMENTAL RESULTS

WAXS Data

Figure 1 collects the WAXS spectra of PVDF- Fe_2O_3 nanocomposites in the two theta range from 5 to 70° . The reflections corresponding to the polymeric matrix (PVDF) and nanofiller (Fe_2O_3) are observed. The lines located at 17° , 18° , 19° , and 26° have been assigned to the α phase of PVDF and identified as representing the reflections of (100), (020), (110), and (021) planes, respectively.^{41–44} The lines at 35° , 43° , 57° , and 63°

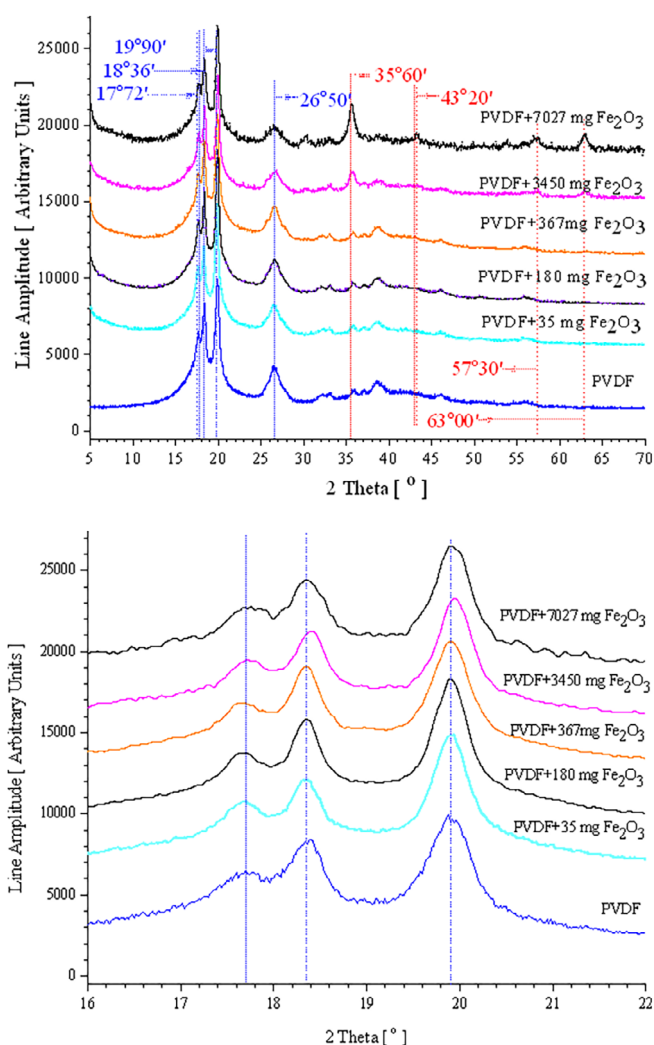


Figure 1. (a) TOP: WAXS spectra of PVDF- Fe_2O_3 nanocomposites. (b) LOW: Details of the region of WAXS spectra assigned to PVDF. [Color figure can be viewed at wileyonlinelibrary.com]

were assigned to (311) (400), (511), and (440) reflections in $\gamma\text{-Fe}_2\text{O}_3$.^{45–47}

The peaks of the nanofiller ($\gamma\text{-Fe}_2\text{O}_3$) are broad and weak, and consequently, it is difficult to estimate accurately the changes occurring within the Fe_2O_3 crystals and crystallites while they are dispersed in the polymeric matrix. However, the first three lines of PVDF allow for a detailed analysis. Each line was individually fitted by a single Lorentzian, in order to estimate accurately the parameters of WAXS spectra. The fitting provided the position, width, and intensity of each WAXS line originating from the polymeric matrix. Only line positions and linewidths were analyzed in detail.

As may be noticed from Figure 2, the positions of the X-ray lines assigned to PVDF are affected by the loading with iron oxide nanoparticles. Qualitatively, the positions of the WAXS lines assigned to (100) and (020) reflections of PVDF show similar behavior, indicating a dilation of the nanofiller's crystalline lattice upon the loading of the PVDF matrix (up to a concentration of about 1% wt nanofiller). By increasing the amount of nanofiller

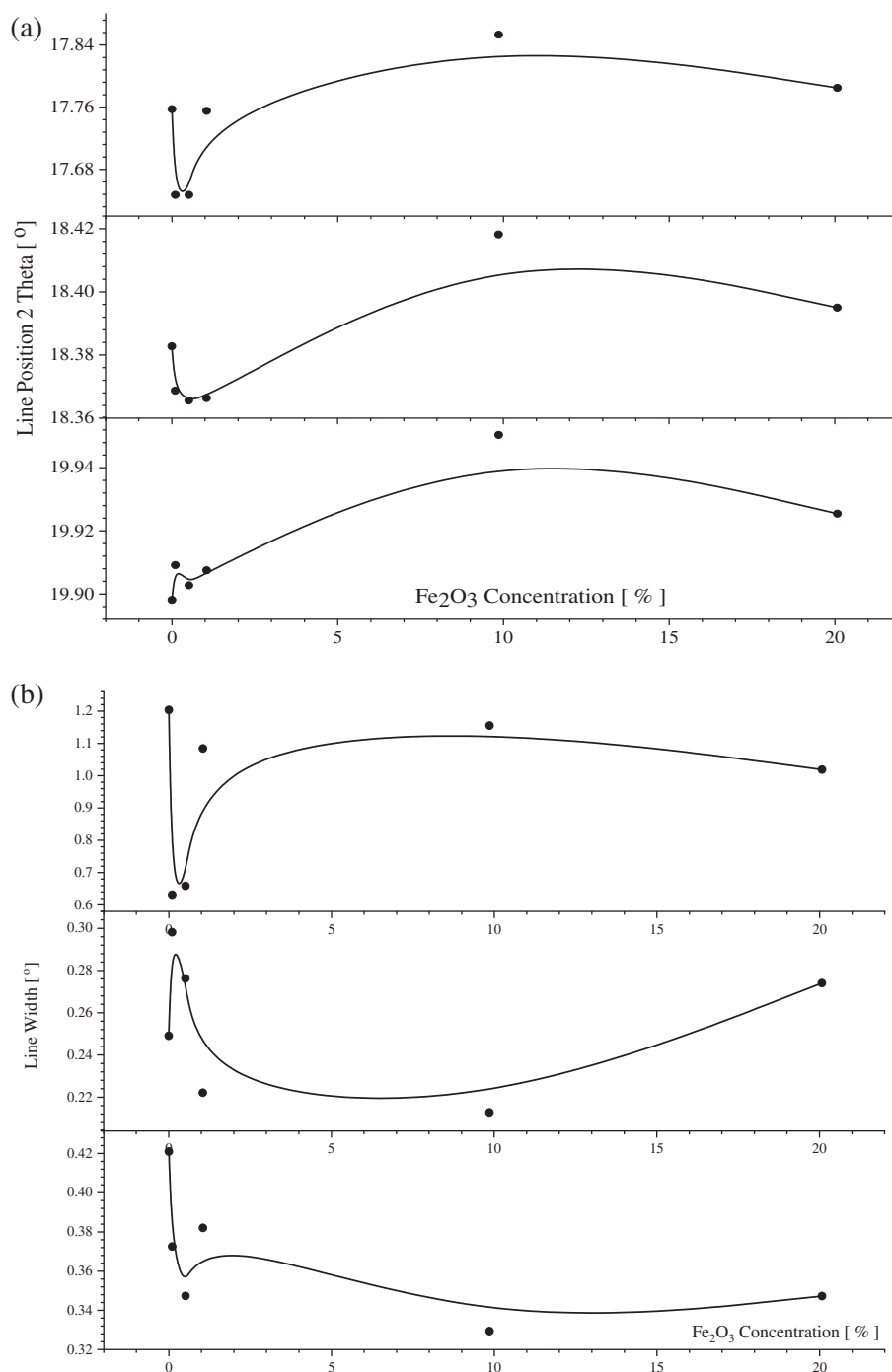


Figure 2. (a) The dependence of the WAXS line position of PVDF on Fe₂O₃ content. (b) The dependence of the WAXS line width of PVDF on Fe₂O₃ content.

from 1% up to about 10% wt, the unit crystal is contracted as the crystallites are subjected to a compressive strain (pressure). Consequently, the [100] and [010] reflections of PVDF are shifted toward the larger two theta values. A weak dilation of the polymeric crystal lattice is again noticed as the concentration of iron oxide is increased from 10 to 20%. Within experimental errors, it is reasonable to conclude that for the [110] reflection, the nanoparticles are compressing the unit crystal as more nanofiller

is added to the polymeric matrix (from 0 to about 10% Fe₂O₃). By further increasing the nanofiller content, the size of the crystal along the [110] direction is increased, as the polymer accommodates for more filler. The small oscillation at low loading with Fe₂O₃ is almost within experimental errors. However, all three reflections are showing a similar dependence of the line position on the loading with Fe₂O₃ (for concentrations of the nanofiller ranging between 1 and 20% wt Fe₂O₃). This analysis reflects the

complex balance of stresses and strains in polymer-based nanocomposites as the polymer matrix tries to accommodate the filler while adjusting to increased strains and stresses.

The lower panel of Figure 2 shows the effect of Fe_2O_3 nanoparticles on the width of the first three reflections assigned to PVDF. As discussed previously, the line width of WAXS line is typically controlled by two parameters; the size of the crystallite along a direction perpendicular to the considered reflection and the stress/strain exerted on the (nano)crystal along the crystalline direction corresponding to the reflection plane. For the [100] and [110] reflections, the linewidth decreases as the content of Fe_2O_3 is increased from 0 to 1%. This suggests a combination of the decrease of the strain exerted on the PVDF crystal and the increase of the size of PVDF crystallites. Combining the data from line position and linewidth dependence on the loading with nanofiller, it is concluded that the governing factor is represented by the size of crystallites. As the Fe_2O_3 concentration is increased from 1 to 10% wt Fe_2O_3 , the linewidth of the polymer matrix crystal is increased. This suggests a decrease in the size of crystallites, competing with an increasing tensile strain exerted on the crystalline matrix. In this case, both the tensile strain and the size of crystallites may compete to explain the actual dependence of linewidth and position on the concentration of nanofiller.

The dependence of the width of the (020) reflection on the loading with the nanofiller is more complex. As the concentration of the nanofiller is increased from 0 to about 1% wt Fe_2O_3 , the linewidth is increasing, suggesting a decrease in the size of crystallites and an increase of the strain. The increase of the strain may be compatible with the shift of the line position, indicating

that both mechanisms may compete to explain the behavior in this domain. Same arguments apply for the range 10 to 20% wt Fe_2O_3 . As the concentration of the nanofiller is increased from 1% up to about 10% wt Fe_2O_3 , the linewidth decreases, suggesting a growth of the size of crystallites and a decreased of the strain (eventually a compression) of the crystal lattice size. By considering both the line position and the linewidth dependence on the nanofiller concentration, it is concluded that the change of the size of crystallites is the dominant mechanism.

The Raman spectra of PVDF- Fe_2O_3 nanocomposites are collected in Figure 3. At low loading with nanofiller, the spectra are dominated by Raman lines originating from the polymeric matrix. Typically, the spectra obtained by the green laser are well resolved in the 3000 cm^{-1} range.

As it is noticed from Table I, the Raman lines of the investigated nanocomposites are dominated by α PVDF (or form III), with eventually a very small admixture of the β PVDF phase. As noticed from Table I, the Raman line of maghemite ($\gamma\text{-Fe}_2\text{O}_3$) located at 790 cm^{-1} is overlapping with one of the strong lines of α PVDF. The Raman lines of Fe_2O_3 at room temperature and low laser powers (of the order of 1 mW) are reported as being weak and broad.⁴⁶ By increasing the laser power, the probability to locally heat the sample and to eventually start the degradation of the polymeric matrix is enhanced. This combination prevented us from obtaining well-resolved Raman spectra of iron oxide.

The lines located at the low Raman position are weak and cannot be accurately fitted. The first Raman line that may be fitted with acceptable accuracy is located at 610 cm^{-1} and was assigned to skeletal CCC scissoring and CF_2 bending and wagging (see

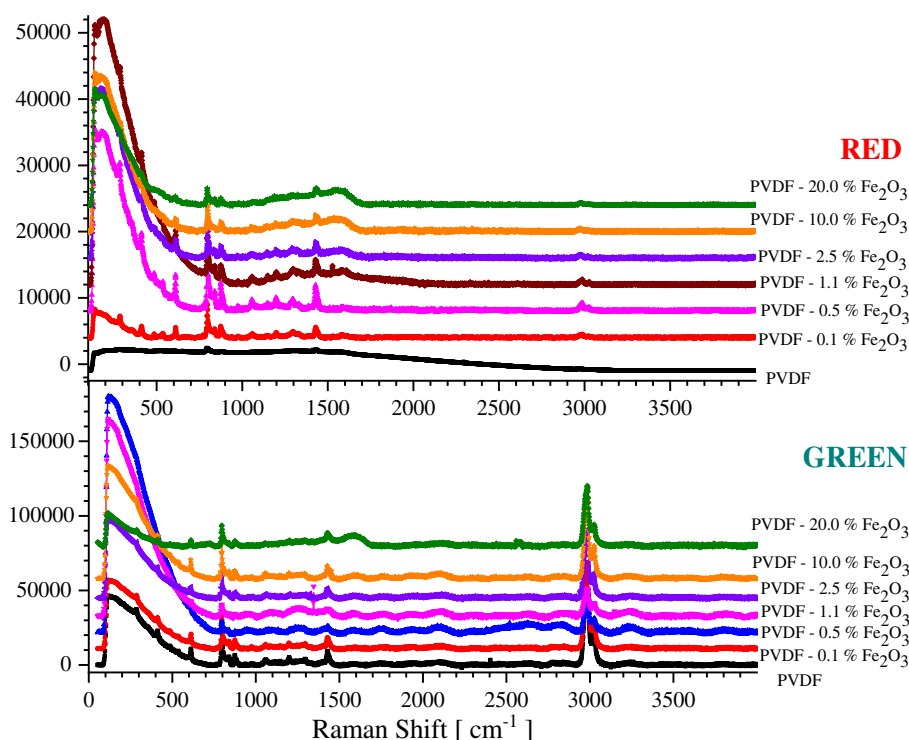


Figure 3. Raman spectra of PVDF- Fe_2O_3 nanocomposites. [Color figure can be viewed at wileyonlinelibrary.com]

Table I. Identification of the Raman Lines Observed in PVDF-Fe₂O₃ Nanocomposites

Position red [cm ⁻¹]	Position green [cm ⁻¹]	Assignment	Reported position [cm ⁻¹]	Reference	Obs
286	286	CF ₂ twist and wagging	284	19	α PVDF
286	286	CF ₂ twist and wagging	287	48	α PVDF
413	413	CF ₂ rocking	410	19	α PVDF
413	413	CF ₂ and CH ₂ rocking	414	48	α PVDF
485	485	CF ₂ scissoring and wagging	484	19	α PVDF
485	485	Combined in phase CF ₂ wagging and bending	485	49	α PVDF
538	538	CF ₂ scissoring	533	19	α PVDF
538	538	CF ₂ bending	537	49	α PVDF
538	538	CF ₂ bending and wagging	545	15	α PVDF
610	610	CF ₂ and CCC scissoring	609	19	α PVDF
610	610	Combined CF ₂ bending and CCC skeletal out of phase vibrations	612	49	α PVDF
610	610	CF ₂ bending and wagging	615	15	α PVDF
797	797	CH ₂ rocking	794	19	α PVDF
797	797	Symmetric CF ₂ stretching characteristic to alpha phase	799	50	α PVDF
797	797	CH ₂ rocking	800	48	α PVDF
840	840	Combined CH ₂ rocking and CF ₂ asymmetric stretching	837	19	α PVDF
840	840	Symmetric CF ₂ stretching characteristic to beta phase	834	50	β-PVDF
840	840	CH ₂ rocking	841	48	α PVDF
878	878	CC symmetric stretching and CCC scissoring	872	19	α PVDF
878	878	CC symmetric stretching and skeletal bending	876	48	α PVDF
878	878	CC and CF ₂ symmetric stretching	881	19	α PVDF
1060	1060	CF ₂ symmetric stretching and CC asymmetric stretching	1058	48	α PVDF
1060	1060	CC asymmetric stretching, CH ₂ wagging	1055	19	α PVDF
1150	1150	CC and CF ₂ symmetric vibrations	1144	19	α PVDF
1150	1150	CF ₂ symmetric and CC antisymmetric vibrations	1150	48	α PVDF
1200	1200	CF ₂ symmetric stretching, CH ₂ wagging	1196	19	α PVDF
1200	1200		1279	51	β-PVDF
1300	1300	CF ₂ symmetric stretching and rocking	1291	19	α PVDF
1300	1300	CF ₂ antisymmetric stretching and rocking	1296	48	α PVDF
1430	1430	CH ₂ deformation and wagging	1432	19	α PVDF
1430	1430	CH ₂ wagging and bending	1430	48	α PVDF
2970	2970	CH ₂ symmetric vibrations	2972	19	α PVDF
2970	2970	CH ₂ symmetric vibrations	2972	48	α PVDF
2990	2990	CH ₂ antisymmetric stretching	2990	48	α PVDF
2990	2990	CH ₂ symmetric vibrations	2985	19	α PVDF
3025	3025	CH ₂ antisymmetric vibrations	3023	19	α PVDF
3025	3025	CH ₂ antisymmetric vibrations	3030	48	α PVDF

Table I). Eventually, this may represent a superposition of two lines assigned to PVDF (see Table I).

The line was fitted by a simple Lorentzian shape. Figure 4 is showing the line located at 610 cm^{-1} (left panel), for various loading by Fe_2O_3 , where the red line represents the outcome of the best fit (for the resonance line) and the filled circles the experimental data. The dependence of the Raman line position and width on the loading with Fe_2O_3 is shown in the right panel of Figure 4.

There is a certain consistency of the WAXS and Raman spectra, as the dependence of the Raman line position on the loading with Fe_2O_3 shows a three-domain behavior, analogous to the position and width dependence of the X-ray spectra on the loading with Fe_2O_3 . The ranges are similar: 0 to 1% Fe_2O_3 , 1 to 10% Fe_2O_3 , and 10 to 20% Fe_2O_3 .

In the first range (for the line located at 610 cm^{-1} ; see Figure 4), as the loading by Fe_2O_3 is increased up to 1% wt, the Raman line position is shifted upward, suggesting compression of the polymeric matrix due to the nanofiller. As the concentration of Fe_2O_3 is increased up to 10% wt Fe_2O_3 , the Raman linewidth, is shifted downward, indicating the stretching of the polymeric matrix due to the increased loading by nanofiller. By further increasing the loading with Fe_2O_3 , above 10% Fe_2O_3 , the position of the Raman line moves downwards, consistent with an expansion (positive strain) of the polymeric matrix.

The next intense and isolated line is located at about 800 cm^{-1} and originates from symmetric CF_2 stretching, eventually combined with some CH_2 rocking characteristic α PVDF (see Figure 5). As in the previous case, the dependence of the Raman

line position on the Fe_2O_3 concentration presents three domains. The first domain reflects what is happening with the polymeric matrix as the content of nanofiller is increased up to 1% wt Fe_2O_3 . The increase of the position of the Raman line is consistent with a negative strain (pressure) acting on the PVDF matrix.

Further increase of the concentration of Fe_2O_3 results in a drop of the line position suggesting that the polymeric matrix is expanded (a positive strain of the polymeric matrix). Nevertheless, the expansion of the polymeric matrix reaches a minimum at about 2.5% nanofiller (not at 10% Fe_2O_3 as in the case of WAXS data). A plateau is eventually noticed in the range of 2.5–10% nanofiller. Further loading with nanofiller results in the upward shift of the Raman line, consistent with a compressive (negative) strain exerted on the nanocomposite before fracture.

Figure 6 shows the dependence of the spectrum at about 2980 cm^{-1} on the loading with Fe_2O_3 . The spectrum in this range has been fitted with a combination of two Lorentzian lines, and the best fit was used to estimate the position, intensity, and width of these lines. The right panel of Figure 6 depicts the dependence of the line position (left, blue) and line width (right, red) on the Fe_2O_3 loading. The two lines are located at about 2976 cm^{-1} and 2987 cm^{-1} , respectively.

The first line reflects CH_2 symmetric vibrations and, respectively CH_2 antisymmetric stretching, see the Table). As may be inferred from Figure 6 (right panel), the position of the line located at 2988 cm^{-1} is almost independent on the loading with nanoparticles up to about 10% wt Fe_2O_3 . Further increase of the concentration of Fe_2O_3 results in the shift of the resonance line downward, compatible with a tensile strain acting on the matrix. The position of the line located at 2982 cm^{-1} is shifted

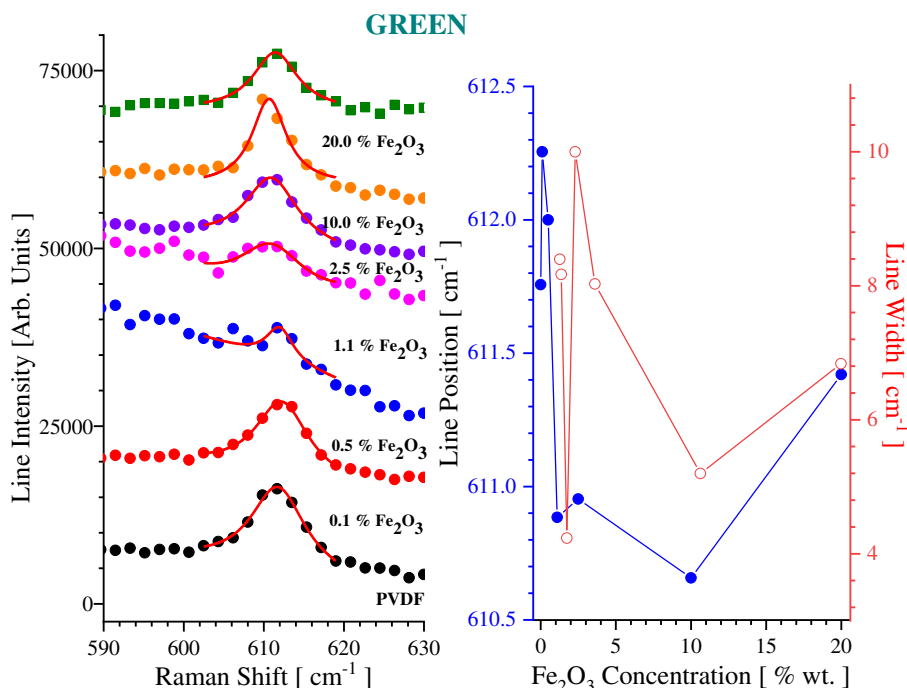


Figure 4. Detail of the Raman line located at 611 cm^{-1} (left) and the dependence of the position and width of the Raman line on Fe_2O_3 concentration (right). [Color figure can be viewed at wileyonlinelibrary.com]

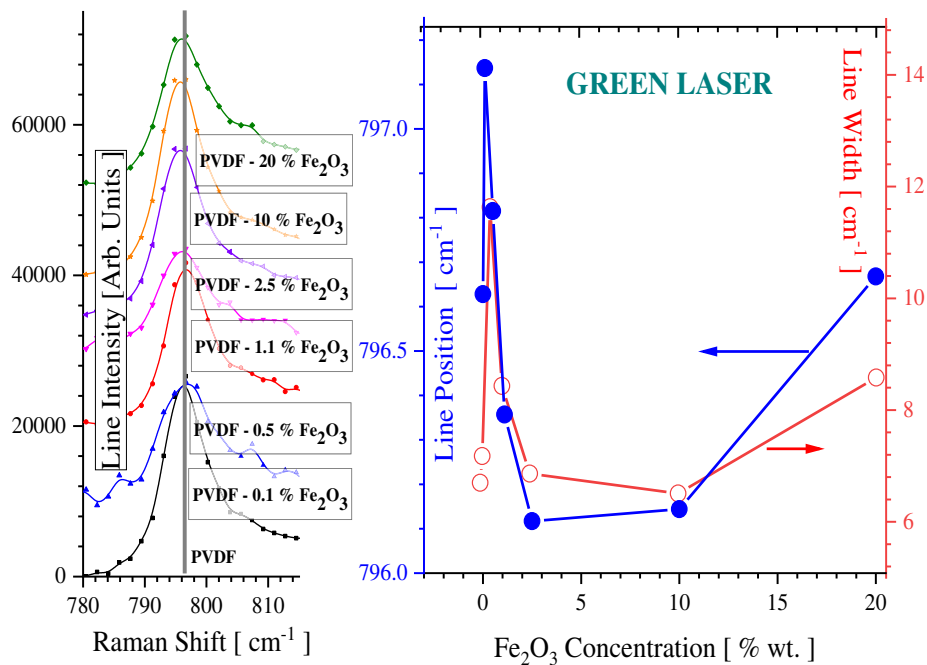


Figure 5. Detail of the Raman line located at 797 cm⁻¹ (left) and the dependence of the position and width of the Raman line on Fe₂O₃ concentration (right). [Color figure can be viewed at wileyonlinelibrary.com]

downwards as the loading with Fe₂O₃ is increased, indicating a positive tensile strain up to about 1% Fe₂O₃. Further increasing the amount of nanofiller from 1 to 10% Fe₂O₃ resulted in an upward shift of the Raman line, consistent with a pressure (negative strain). Finally, by increasing the concentration of Fe₂O₃ from 10 to 20% Fe₂O₃, the position of this line is shifted downward, indicating a tensile strain acting on the polymeric matrix.

The line located at 3020 cm⁻¹ is assigned to CH₂ antisymmetric vibrations; the dependence of its parameters on the loading with Fe₂O₃ is shown in the right panel of Figure 7. The position of this line is displaced towards smaller Raman shifts as the loading with Fe₂O₃ is increased, indicating that the polymeric matrix is subjected to a positive strain (elongation). However, large oscillations of the position of this line were noticed.

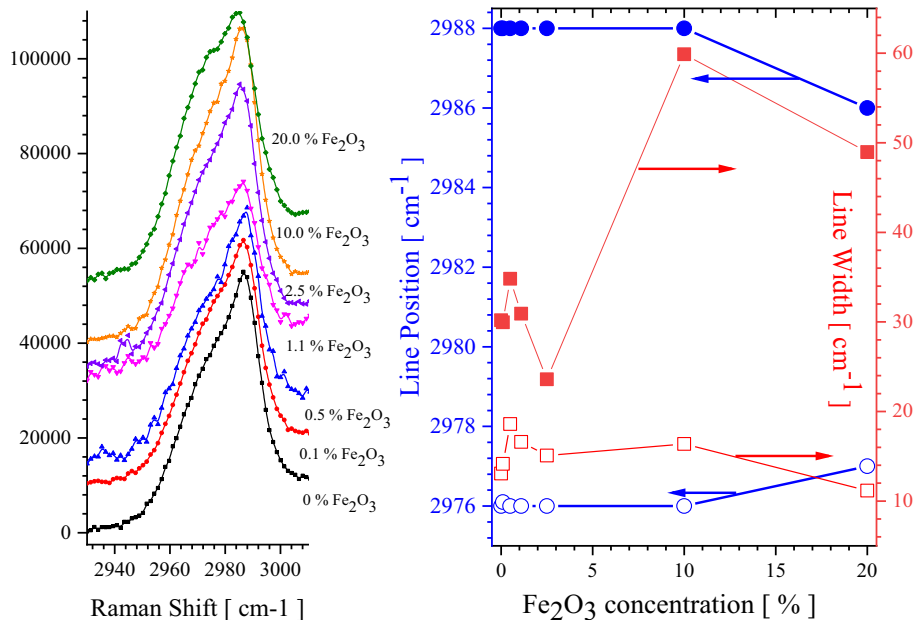


Figure 6. Detail of the Raman spectrum located at 2980 cm⁻¹ (left) and the dependence of the position and width of the Raman line on Fe₂O₃ concentration (right). [Color figure can be viewed at wileyonlinelibrary.com]

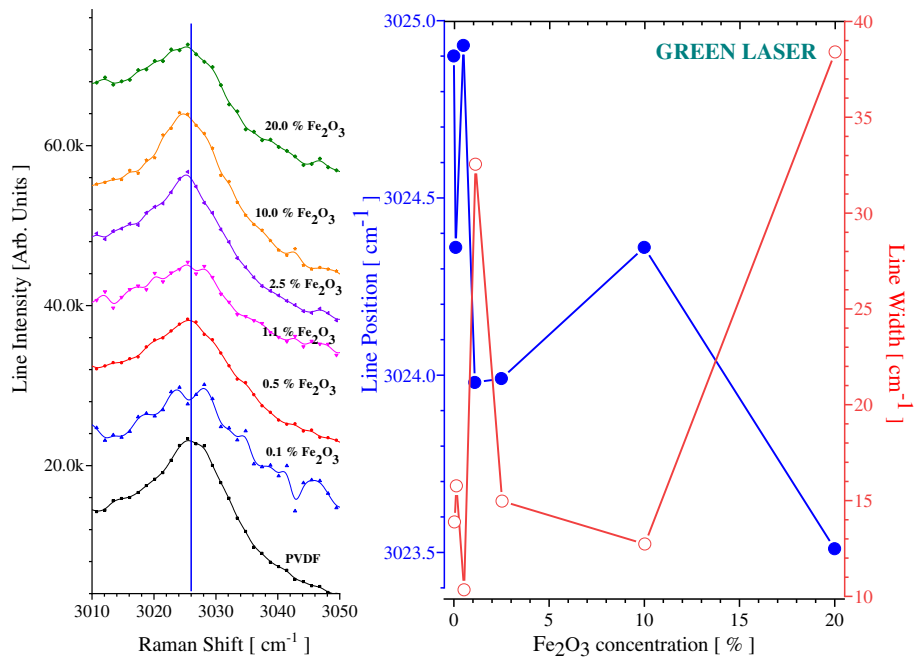


Figure 7. Detail of the Raman spectrum located at 3020 cm⁻¹ (left) and the dependence of the position and width of the Raman line on Fe₂O₃ concentration (right). [Color figure can be viewed at wileyonlinelibrary.com]

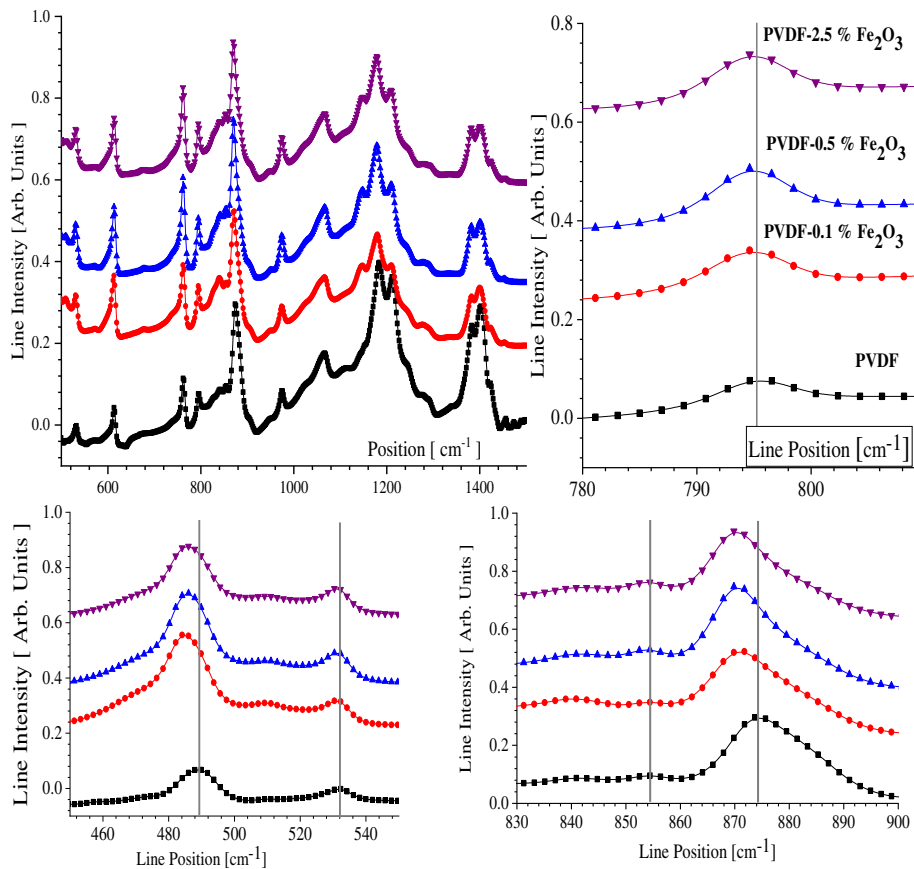


Figure 8. FTIR spectra of some PVDF-Fe₂O₃ nanocomposites. [Color figure can be viewed at wileyonlinelibrary.com]

FTIR data on PVDF loaded by various amounts of Fe_2O_3 are included in Figure 8. Important modifications are noticed at about 1200 cm^{-1} , where CF_2 stretching of rocking motions is expected.⁵³ Such changes may not affect the local polarizability as the Raman spectra in this range are not affected by the loading with Fe_2O_3 . It is noticed that upon loading with maghemite, some FTIR lines are shifted while some others are not significantly affected. This is typical behavior, observed also in the Raman investigations of these samples indicating that for both vibrational spectroscopies, the applied stress or strain's effects are differential, that is, different atomic/molecular motions are affected in different ways.

Large (FTIR) shifts upon the loading with the nanofillers were noticed for the line located at 489 cm^{-1} assigned to the CF_2 scissoring⁵³ motions in α PVDF,⁵⁴ and for the line located at 875 cm^{-1} , assigned to C–C stretching in α PVDF.⁵³ As seen from Figure 8, significantly weaker effects of the loading with Fe_2O_3 nanoparticles were noticed for the FTIR lines located at 530 (assigned to CF_2 bending⁵⁴), 795 (assigned to CH_2 rocking⁵⁴), and 855 (assigned to CH out of the plane deformation⁵⁴) cm^{-1} .

DISCUSSIONS

The research described went beyond most spectroscopic research on polymer-based nanocomposites, focusing on the effect of nanofiller on the parameters of both vibrational (Raman and FTIR) and WAXS spectroscopies. Most important lines have been fitted by Lorentzian line shapes by using the Origin C capabilities, and the best parameters have been reported and analyzed in detail. For all experimental data, the analysis was focused on the line position and linewidth. The reduced number of experimental data in the case of vibrational spectroscopies data (of the order of 10 per spectrum) limited the detailed analysis of the line shape. Further improvements of the next generation of Raman spectrometers will allow us to address this issue and to obtain a full deconvolution of all lines' parameters.

Many physical properties of polymer-based nanocomposites are controlled by surface and volume rather than by mass; consequently, owing to the high density of the nanofiller, a loading by 20% wt Fe_2O_3 of the polymeric matrix expresses an additional increase of about 7% volume for the nanocomposite.

WAXS data confirmed the loading of the polymeric matrix by the nanopowder. However, due to the weak, broad, and noisy signal originating from nanoparticles, solely the lines corresponding to the polymeric matrix were studied in detail. The analysis was focused on the first three most intense lines of the spectrum.

The dependence of the WAXS line positions on the concentration of Fe_2O_3 is qualitatively identical for all three reflections investigated, as the loading with nanofiller is increased from 1 to 20% wt.

The dependence of the positions of the lines corresponding to [100] and [020] reflections on the loading with Fe_2O_3 show a three domain pattern, consistent with the weak increase of the size of the unit crystal as the loading with Fe_2O_3 is increased from 0 to 1%. As the concentration of the nanofiller is increased

(from 0.1% up to 10% wt Fe_2O_3), the lattice distances corresponding to these reflections are decreased, indicating a compression of the polymeric matrix due to the addition of the nanofiller. Further increase of the Fe_2O_3 (from 10 to 20% wt Fe_2O_3) is consistent to a tensile strain (associated with an increase of the corresponding lattice size), which may extend in the very first part of the failing region for this nanocomposite.

The dependence of the positions of [021] reflection on the loading with Fe_2O_3 is more complex. However, the "oscillatory" behavior noticed at low Fe_2O_3 is almost within experimental errors, and essentially two domains were noticed for the dependence of the position of this line on Fe_2O_3 loading. At low Fe_2O_3 concentrations (10% Fe_2O_3 or smaller) the lattice is compressed as the loading with nanofiller is increased. Further increase of the nanofiller's concentration results in a contraction of the crystal lattice, probably as cracking is initiated.

The dependence of the width of the WAXS reflections on the loading by Fe_2O_3 also shows a three-domain structure. In this case the dependence of the line width for the reflections [100] and [110] on the loading by Fe_2O_3 is similar: In the first range (0–1% wt Fe_2O_3) and third range (10–20% wt Fe_2O_3) there is a competition between the decreasing strain and the growth of the size of crystallites as the loading with nanofiller is increased. This suggests for the [100 reflections] that the actual linewidth dependence on Fe_2O_3 loading is controlled by one (or a combination of the two) contributions: smaller strains' acting on the crystal and/or increase of the crystallite's size as the loading with nanoparticles is increased. In this range of concentrations, the line position dependence on the nanofiller concentration is consistent with an increase of the crystal size. In conclusion, the crystalline domain size is governing the dependence of the linewidth on Fe_2O_3 concentration. In the range of 1–10% wt Fe_2O_3 , the linewidth dependence on nanofiller's concentration indicates a decrease in the size of crystallites and an increase of the strain acting on the PVDF crystal. As the increase of the strain is not consistent with the observed dependence of this line position versus the Fe_2O_3 concentration (decrease of the lattice parameters), it is concluded that for this range of concentrations, the X-ray line is controlled by the size of crystallites.

The dependence of the linewidth associated with the [020] reflection on Fe_2O_3 concentration is a "mirror-like" functional dependence compared to the dependence of the [020] line position on Fe_2O_3 loading. In the first range (0–1% Fe_2O_3), the strain exerted on the crystal is increased while the size of crystallites is decreasing. As the increased strain is not consistent with a smaller lattice parameter, it is concluded that in this case the size of crystallites is dominating the dependence of this linewidth on the concentration of nanofiller.

The general concept that the loading with the nanofiller is stretching the polymeric matrix was confirmed by the reported displacement of some Raman and/or FTIR lines as a function of the concentration of the nanofiller. The differential shift of Raman lines will further provide information regarding the contribution of various vibrations and molecular motions to the overall macroscopic mechanical features of the polymer-based nanocomposite. It was shown that the Raman spectra are affected

by the wavelength of the impinging electromagnetic radiation and that various molecular/atomic motions behave differently upon loading with nanofiller or changing the laser source (wavelength).

The Raman line located at 610 cm^{-1} originates from combined CF_2 bending and CCC skeletal out of phase vibrations. Due to the contributions of skeletal vibrations, it is expected that this line would be sensitive to the loading with Fe_2O_3 . The change of the position of this line as the loading with nanoparticles is increased, indicates three domains, consistent with the interpretation of WAXS lines. The first domain, at low content of nanofiller, indicates a positive (compressive strain) acting along the polymeric backbone as the concentration of Fe_2O_3 is increased. By increasing further the loading with Fe_2O_3 , it is noticed that the position of the Raman line is shifted downward, consistent with an expansion behavior, generated by the addition of nanoparticles. Finally, increasing the concentration of Fe_2O_3 from 10 to 20% wt, the line position is shifted upwards suggesting a negative strain (compression) resulting from the crowding of the nanofiller above the elastic capabilities of the matrix. The observed behavior by Raman is not matching the WAXS behavior, indicating that while the WAXS behavior is related to the crystalline component of the polymeric matrix, the Raman behavior is controlled by the amorphous component of the polymeric matrix.

The Raman spectrum at about 800 cm^{-1} was assigned to CH_2 rocking and CF_2 symmetric stretching. It is expected that this line is less sensitive to the presence of the nanofiller. Technically, the dependence of the position of this line on the loading by Fe_2O_3 exhibit the same three-domain behavior (although a “plateau” region may be speculated between 15 and 50% wt Fe_2O_3). As the Fe_2O_3 concentration is increased from 0 to 1% wt Fe_2O_3 , the displacement of this line to a higher position reflects a compressive strain.

The spectrum recorded at about 2980 cm^{-1} was deconvoluted into two Lorentzian lines and fitted as a pair. These lines are assigned to CH_2 symmetric vibrations. The line located at 2980 cm^{-1} shows the three-domain behavior, compatible with an increasing elongational strain/stress as the loading is increased (at very low and very large concentration of nanoparticles). The other line located at 2988 cm^{-1} is almost not affected by the loading with Fe_2O_3 as the loading is increased up to about 10% wt Fe_2O_3 . By increasing the concentration of Fe_2O_3 above 10%, the contribution of the elongational strain becomes visible. This may suggest that the line recorded at 2988 cm^{-1} is eventually connected with the crystalline domains of PVDF and that their destruction starts at loadings above 10% wt Fe_2O_3 . At lower concentration with nanofiller, the amorphous component of the polymer is accommodating for the nanoparticles.

CONCLUSIONS

- WAXS data revealed important modifications within the crystalline polymeric matrix due to the addition of Fe_2O_3 nanoparticles.
- Unfortunately, the WAXS spectra of Fe_2O_3 were not well resolved to allow for a detailed analysis on the effect of the polymeric matrix on the nanofiller.

- The same behavior was noticed for the Raman spectra of PVDF- Fe_2O_3 nanocomposites for both green and red excitations, that is, the Raman spectra of PVDF- Fe_2O_3 nanocomposites are dominated by the Raman lines assigned to the polymeric matrix (PVDF). However, there are significant differences between the Raman spectra obtained by using red and respectively green lasers. It appears that line intensities are the most affected parameters, with no significant change of the positions of Raman lines using red and green excitations. This suggests that the polymeric Raman lines are essentially not dispersive. The conclusion is further supported by the agreement between the positions of the lines allowed both in Raman and FTIR spectroscopy, which are not showing significant displacements of their position.
- Both WAXS, Raman, and FTIR data indicated that the polymeric matrix is dominantly represented by the α phase of PVDF.
- WAXS data confirmed the presence of nanoparticles; the recorded reflections are consistent with γ phase Fe_2O_3 (maghemite).
- Typically, the dependence of the line position on the loading by Fe_2O_3 is represented by three domains, one ranging between 0 and 1.0% wt Fe_2O_3 , the second between 1.0 and 10% wt Fe_2O_3 , and the last between 10 and 20% wt Fe_2O_3 .
- It is suggested that the Fe_2O_3 nanoparticles are preferentially located within the amorphous domains as their concentration is increased from 0 to 10% wt. By increasing the concentration of Fe_2O_3 nanoparticles from 10 to 20% wt, it was noticed that the nanoparticles start to disrupt the crystalline phase.
- The relative stretching is not very large, as the highest loading with Fe_2O_3 requires just an increase by 7% of the volume of the polymer to accommodate for the nanofiller. Studies at higher concentration of nanofiller may be of particular importance and the “bleeding regime” where the polymeric matrix starts to loose the nanofiller, due to the collapse of its elastic features will provide additional information.

Finally, it is important to stress on the potential connections between WAXS and Raman/FTIR data. The WAXS linewidth is controlled by both size of the crystallites and local stress/strains. The classical theta—two theta recording of experimental data assumes a random distribution of crystallites and does not provide sufficient information to deconvolute these two contributions (crystallite size and local stress). It is expected that after the next refinement of Raman spectroscopy (which will include a calibration of the displacement of the Raman lines versus the applied uniaxial stress) a more detailed understanding of the WAXS line width, will result due to the combined analysis of WAXS/FTIR/Raman spectra. At this point, the manuscript added qualitative arguments and connections that justifies this description, providing a potential path for such evolution.

ACKNOWLEDGMENTS

Authors acknowledge the Department of Defense Grant “Raman Spectrometer for the Characterization of Advanced Materials and Nanomaterials,” W911NF-15-1-0063, the NSF DMR-1523577: UTRGV-UMN Partnership for Fostering Innovation by Bridging Excellence in Research and Student Success.

REFERENCES

- Salimi, A.; Yousefi, A. A. *J. Polym. Sci. Part B Polym. Phys.* **2004**, *42*, 3487. <https://doi.org/10.1002/polb.20223>.
- Pramoda, K. P.; Mohamed, A.; Phang, I. Y.; Liu, T. *Polym. Int.* **2005**, *54*, 226. <https://doi.org/10.1002/pi.1692>.
- He, X.; Yao, K. *Appl. Phys. Lett.* **2006**, *89*, 1. <https://doi.org/10.1063/1.2352799>.
- Kochervinskii, V. V. *Crystallogr. Rep.* **2003**, *48*, 649. <https://doi.org/10.1134/1.1595194>.
- Nan, C. W.; Bichurin, M. I.; Dong, S.; Viehland, D.; Srinivasan, G. *J. Appl. Phys.* **2008**, *103*, 031101. <https://doi.org/10.1063/1.2836410>.
- Nan, C.; Cai, N.; Liu, L.; Zhai, J.; Ye, Y.; Lin, Y. *J. Appl. Phys.* **2003**, *94*, 5930. <https://doi.org/10.1063/1.1614866>.
- Andrew, J. S.; Starr, J. D.; Budi, M. A. K. *Scr. Mater.* **2014**, *74*, 38. <https://doi.org/10.1016/j.scriptamat.2013.09.023>.
- Lebedev, S. M.; Gefle, O. S. Influence of prehistory on properties of PVDF films. In Proc. 2012 7th Int. Forum Strateg. Technol. IFOST 2012; IEEE: Red Hook, New York, **2012**; p 1. <https://doi.org/10.1109/IFOST.2012.6357799>.
- Patro, T. U.; Mhalgi, M. V.; Khakhar, D. V.; Misra, A. *Polymer (Guildford)*. **2008**, *49*, 3486. <https://doi.org/10.1016/j.polymer.2008.05.034>.
- Sencadas, V.; Lanceros-Méndez, S.; Sabater, R.; Serra, I.; Andrio Balado, A.; Gómez Ribelles, J. L. *Eur. Phys. J. E.* **2012**, *35*, 41. <https://doi.org/10.1140/epje/i2012-12041-x>.
- Hendra, P. J.; Stratton, P. M. *Chem. Rev.* **1969**, *69*, 325. <https://doi.org/10.1021/cr60259a003>.
- Snyder, R. G. *J. Mol. Spectrosc.* **1970**, *36*, 222. [https://doi.org/10.1016/0022-2852\(70\)90106-2](https://doi.org/10.1016/0022-2852(70)90106-2).
- Tashiro, K.; Kobayashi, M.; Tadokoro, H. *Macromolecules.* **1981**, *14*, 1757. <https://doi.org/10.1021/ma50007a028>.
- Ali, N.; Chipara, D.; Lozano, K.; Hinthorne, J.; Chipara, M. *Appl. Surf. Sci.* **2017**, *421*, 220. <https://doi.org/10.1016/j.apsusc.2016.11.166>.
- Pradhan, S. K.; Kumar, A.; Sinha, A. N.; Kour, P.; Pandey, R.; Kumar, P.; Kar, M. *Ferroelectrics.* **2017**, *516*, 18. <https://doi.org/10.1080/00150193.2017.1362243>.
- Chipara, D. M.; Macossay, J.; Ybarra, A. V. R.; Chipara, A. C.; Eubanks, T. M.; Chipara, M. *Appl. Surf. Sci.* **2013**, *275*, 23. <https://doi.org/10.1016/j.apsusc.2013.01.116>.
- Liao, C. C.; Hou, S. S.; Wang, C. C.; Chen, C. Y. *Polymer (Guildford)*. **2010**, *51*, 2887. <https://doi.org/10.1016/j.polymer.2010.04.046>.
- Sajkiewicz, P.; Wasiak, A.; Gocl, Z. *Eur. Polym. J.* **1999**, *35*, 423.
- Constantino, C. J. L. L.; Job, A. E.; Simões, R. D.; Giacometti, J. A.; Zucolotto, V.; Oliveira, O. N.; Gozzi, G.; Chinaglia, D. L.; Job, A. E.; Simões, R. D.; Gozzi, G.; Giacometti, J. A.; Zucolotto, V.; Constantino, C. J. L. L. *Appl. Spectrosc.* **2005**, *59*, 275. <https://doi.org/10.1366/0003702053585336>.
- Qin, F.; Lei, Z.; Ma, Y.; Fang, Q.; Bai, R.; Qiu, W.; Yan, C.; Feng, Y. *Compos. Part A Appl. Sci. Manuf.* **2018**, *112*, 134. <https://doi.org/10.1016/j.compositesa.2018.06.002>.
- Fina, L. J.; Bower, D. I.; Ward, I. M. *Polymer (Guildford)*. **1988**, *29*, 2146. [https://doi.org/10.1016/0032-3861\(88\)90105-X](https://doi.org/10.1016/0032-3861(88)90105-X).
- Rusli, R.; Shanmuganathan, K.; Rowan, S. J.; Weder, C.; Elchhorn, S. J. *Biomacromolecules.* **2010**, *11*, 762. <https://doi.org/10.1021/bm1001203>.
- Chipara, D. M.; Panaitescu, D. M.; Lozano, K.; Nicolae, R. A. G. C. A.; Chipara, M. *Polymer (Guildford)*. **2019**, *176*, 74. <https://doi.org/10.1016/j.ygyno.2016.04.081>.
- Anagnostopoulos, G.; Androulidakis, C.; Koukaras, E.; Tsoukleri, G. N.; Polyzos, I.; Parthenios, J.; Papagelis, K.; Galiotis, C. *Appl. Mater. Interfaces.* **2015**, *7*, 4216. <https://doi.org/10.1021/am508482n>.
- Colomban, P. *Adv. Nat. Sci. Nanosci. Nanotechnol.* **2013**, *4*, 013001. <https://doi.org/10.1088/2043-6262/4/1/013001>.
- Chipara, M.; Hamilton, J.; Chipara, A. C. A. C.; George, T.; Chipara, D. M. D. M.; Ibrahim, E. E. E. E.; Lozano, K.; Sellmyer, D. J. D. J. *J. Appl. Polym. Sci.* **2012**, *125*, 353. <https://doi.org/10.1002/app>.
- Chipara, M.; Jones, B.; Chipara, D. M.; Li, J.; Lozano, K.; Valloppilly, S.; Sellmyer, D. *E-Polymers.* **2017**, *17*, 303. <https://doi.org/10.1515/epoly-2016-0286>.
- Rueda, D. R.; Garcia Gutiérrez, M. C.; Ania, F.; Zolotukhin, M. G.; Balta Calleja, F. J. *Macromolecules.* **1998**, *31*, 8201.
- Gregorio, R. *J. Appl. Polym. Sci.* **2006**, *100*, 3272. <https://doi.org/10.1002/app.23137>.
- Dillon, D. R.; Tenneti, K. K.; Li, C. Y.; Ko, F. K.; Sics, I.; Hsiao, B. S. *Polymer (Guildford)*. **2006**, *47*, 1678. <https://doi.org/10.1016/j.polymer.2006.01.015>.
- Krishna Bama, G.; Indra Devi, P.; Ramachandran, K. *J. Mater. Sci.* **2009**, *44*, 1302. <https://doi.org/10.1007/s10853-009-3271-8>.
- Priya, L.; Jog, J. P. *J Polym Sci B.* **2003**, *41*, 31.
- Khorsand Zak, A.; Abd. Majid, W. H.; Abrishami, M. E.; Yousefi, R. *Solid State Sci.* **2011**, *13*, 251. <https://doi.org/10.1016/j.solidstatesciences.2010.11.024>.
- Tarantili, P. A.; Andreopoulos, A. G.; Galiotis, C. *Macromolecules.* **1998**, *31*, 6964. <https://doi.org/10.1021/ma961498l>.
- Nakamoto, S.; Tashiro, K.; Matsumoto, A. *Macromolecules.* **2003**, *36*, 109. <https://doi.org/10.1021/ma021090q>.
- Zhao, Q.; Wagner, H. D. *Compos. Part A Appl. Sci. Manuf.* **2003**, *34*, 1219. <https://doi.org/10.1016/j.compositesa.2003.07.005>.
- De la Vega, A.; Kinloch, I. A.; Young, R. J.; Bauhofer, W.; Schulte, K. *Compos. Sci. Technol.* **2011**, *71*, 160. <https://doi.org/10.1016/j.compscitech.2010.11.004>.
- Lucas, M.; Young, R. J. *Compos. Sci. Technol.* **2004**, *64*, 2297. <https://doi.org/10.1016/j.compscitech.2004.01.021>.
- Young, R. J.; Eichhorn, S. J. *Polymer (Guildford)*. **2007**, *48*, 2. <https://doi.org/10.1016/j.polymer.2006.11.016>.
- Wagner, H. D.; Amer, M. S.; Schadler, L. S. *Appl. Compos. Mater.* **2000**, *7*, 209. <https://doi.org/10.1023/A:1008956929081>.
- Mago, G.; Kalyon, D. M.; Fisher, F. T. *J. Nanomater.* **2008**, *2008*, 1. <https://doi.org/10.1155/2008/759825>.

42. Gao, K.; Hu, X.; Dai, C.; Yi, T. *Mater. Sci. Eng. B Solid State Mater. Adv. Technol.* **2006**, *131*, 100. <https://doi.org/10.1016/j.mseb.2006.03.035>.
43. Tiwari, V.; Srivastava, G. *J. Polym. Res.* **2014**, *21*, 587. <https://doi.org/10.1007/s10965-014-0587-0>.
44. Sekar, R.; Tripathi, A. K.; Pillai, R. K. C. *Mater. Sci. Eng. B.* **1989**, *5*, 33. [https://doi.org/10.1016/0921-5107\(89\)90302-4](https://doi.org/10.1016/0921-5107(89)90302-4).
45. Sahoo, S. K.; Agarwal, K.; Singh, A. K.; Polke, B. G.; Raha, K. C. *Sci. Technol.* **2010**, *2*, 118. <https://doi.org/10.4314/ijest.v2i8.63841>.
46. El Mendili, Y.; Bardeau, J. F.; Randrianantoandro, N.; Gourbil, A.; Greneche, J. M.; Mercier, A. M.; Grasset, F. *J. Raman Spectrosc.* **2011**, *42*, 239. <https://doi.org/10.1002/jrs.2762>.
47. Islam, M. S.; Abdulla-Al-Mamun, M.; Kurawaki, J.; Kusumoto, Y.; Bin Mukhlis, M. Z. *J. Sci. Res.* **2012**, *4*, 99. <https://doi.org/10.3329/jsr.v4i1.8727>.
48. Kobayashi, M.; Tashiro, K.; Tadokoro, H. *Macromolecules.* **1974**, *8*, 158.
49. Mattsson, B.; Ericson, H.; Torell, L. M.; Sundholm, F. *Polym. Sci. Part A Polym. Chem.* **1999**, *37*, 3317.
50. Zhou, X.; Cakmak, M. *J. Macromol. Sci. Part B Phys.* **2007**, *46*(B), 667. <https://doi.org/10.1080/00222340701388680>.
51. Sengupta, D.; Kottapalli, A. G. P.; Chen, S. H.; Miao, J. M.; Kwok, C. Y.; Triantafyllou, M. S.; Warkiani, M. E.; Asadnia, M. *AIP Adv.* **2017**, *7*, 105205. <https://doi.org/10.1063/1.4994968>.
52. Cherian, C. T.; Sundaramurthy, J.; Kalaivani, M.; Ragupathy, P.; Kumar, P. S.; Thavasi, V.; Reddy, M. V.; Sow, C. H.; Mhaisalkar, S. G.; Ramakrishna, S.; Chowdari, B. V. R. *J. Mater. Chem.* **2012**, *22*, 12198. <https://doi.org/10.1039/c2jm31053h>.
53. Constantino, C. J. L.; Job, A. E.; Simões, R. D.; Giacometti, J. A.; Zucolotto, V.; Oliveira, O. N.; Gozzi, G.; Chinaglia, D. L. The investigation of $\alpha \rightarrow \beta$ phase transition in poly(vinylidene fluoride) (PVDF). In Proc. Int. Symp. Electrets; IEEE: Red Hook, New York, **2005**; p 178. <https://doi.org/10.1109/ise.2005.1612350>.
54. Bormashenko, Y.; Pogreb, R.; Stanevsky, O.; Bormashenko, E. *Polym. Test.* **2004**, *23*, 791. <https://doi.org/10.1016/j.polymertesting.2004.04.001>.